Sensors & Transducers, Vol. 171, Issue 5, May 2014, pp. 134-140

Sensors & Transducers

Constructing Gyro-free Inertial Measurement Unit from Dual Accelerometers for Gesture Detection

[1] Xiangluo WANG, [2] Chunlei YANG
[1] Dept. of Information Technology, Luoyang Normal University,
71 Longmen Road, Luoyang, 471022, China
[2] Dept. of Information Engineering, Henan University of Science and Technology,
263 Kaiyuan Road, Luoyang, 471023, China
[1] Tel.: (+86)15937918076
[1] E-mail: kevinx.walter@gmail.com

Received: 28 April 2014 /Accepted: 27 May 2014 /Published: 31 May 2014

Abstract: Inertial measurement unit for gesture-based interface is characterized by short sampling time and lower cumulative errors, which indicates that MEMS sensors are suitable for gesture motion detection. This paper presents a configuration scheme of gyro-free micro inertial measurement unit based on dual MEMS accelerometers, and corresponding methods for calculating angular rates and linear accelerations. The unit is constructed from two triaxial MEMS accelerometers with the near-symmetrical layout; two-value solution space of angular rates can be obtained by differential method, by introducing an energy function, the optimum estimation of angular rates can be achieved by solving a convex optimization problem related to function regression; for raising accuracy, Kalman filtering method is used for denoising arguments by defining proper state & observation equations. The unit is small and comparatively easy to hold for its near-symmetrical structure along major axis; corresponding algorithm is free from cumulative errors and easy for implementation. The simulation results show that the scheme and related algorithms are feasible and effective.

Keywords: Gesture detection, Inertial measurement, Gyro-free, MEMS accelerometer, Function regression, Kalman filtering.

1. Introduction

Differing from existing two-dimensional interaction methods and devices [1] such as keyboards, electronic writing pads, touch screens, and so on, gesture-based interaction technologies can fulfill input tasks well by several steps: sampling angular rates and linear acceleration of the hand-held unit, calculating gesture traces, and pattern recognition [2, 3]. As it is physical and tangible, corresponding researches are becoming much more active.

One of the key steps in gesture interaction is calculating the ground accelerations (relative to gravity) according to gyroscope and accelerometer outputs (relative to the unit itself), and this task can be fulfilled based on inertial navigation technology. Today, familiar schemes of inertial measurement unit include 1) the combinational one which consists of both accelerometer and gyro [4], and 2) the simplified one composed of single accelerometer [5]. Because MENS gyroscopes have larger random drift errors and poor shock resistance ability, and can not meet the large angular rate measuring requirements,

so the first scheme is not always reliable. Meanwhile, the second one has drawbacks such as: gesture regions are strictly limited, and the gesture motions are not very flexible.

Since DiNapoli and Schuler presented gyro-free methods for angular rates measurement in 1965 [6, 7], theories and techniques of gyro-free inertial navigation have been studied widely. Recently, a lot of researches about navigation systems, gesture and human motion patterns recognition are carried out. Among them, six and nine accelerometers configurations, as described in papers of S. J. Merhav, Alfred R. Schuler, Lee Souchen, and Liu Cheng-Yu [8, 9], are most representative. But considering the limited size of measurement units, these schemes are not suitable for gesture-based interactions yet, because of the complicated spatial layout of accelerometers [10]. Meanwhile there is a simplified scheme characterized by three-accelerometers and estimating angular rates through interpolation calculation [11, 12]. From lack of valid learning samples, it should be unfeasible when gesture varies largely.

In his paper, we focus constructing the gyro-free inertial measurement unit from two triaxial MEMS accelerometers, and how to get the primitive features of gestures such as angular rates and linear accelerations with respect to ground. The characteristics of involved methods are as follows: 1) employing MEMS accelerometers rather than gyro to achieve the primitive features of gestures, and accordingly increasing the reliability as well as reducing costs; 2) with reasonable accuracy and efficiency, the unit is easy to hold because of accelerometers' near-symmetrical layout.

2. Principles of Inertial Measurement

When hand-held unit moves in some writing plane with gestures, rotational and translational motions are involved in this process, which can be sensed by inertial components. Normally, Angular rates and composite accelerations are measured using gyro and accelerometer respectively, but an alternative approach exists: using several accelerometers as the substitute for gyro to calculate the angular rates and then achieving ground accelerations of the unit.

Regarding the hand-held unit as a rigid body, and attaching the body frame ($O_bX_bY_bZ_b$) to which, then the following radius vector equation is satisfied for any point P in the unit:

$$\boldsymbol{R}' = \boldsymbol{R} + \boldsymbol{L}, \tag{1}$$

where $\boldsymbol{L}$ and $\boldsymbol{R}'$ are the radius vector of P relative to origins of body frame and inertial frame ($O_eX_eY_eZ_e$) respectively, $\boldsymbol{R}$ is the radius vector between origins of inertial and body frames.

Differentiating this expression twice, and using the theorem of Coriolis, we have,

$$\frac{d_e^2\boldsymbol{R}'}{dt^2} = \frac{d_e^2\boldsymbol{R}}{dt^2} + \frac{d_e\boldsymbol{\omega}}{dt^2}\times\boldsymbol{L} + \boldsymbol{\omega}\times(\boldsymbol{\omega}\times\boldsymbol{L}), \tag{2}$$

where $\frac{d_e^2\boldsymbol{R}'}{dt^2}$ and $\frac{d_e^2\boldsymbol{R}}{dt^2}$ represent the acceleration at point P and the rotation center in the order given, $\frac{d_e\boldsymbol{\omega}}{dt}$ and $\boldsymbol{\omega}$ are the body's angular acceleration and turn rate respectively.

For constructing gyro-free inertial measurement unit, we can mount more than one three-axis accelerometers at different positions of it, the same amount of equations just like eqn. (2) can be established simultaneously, which are expected to provide supports for calculating $\boldsymbol{\omega}$ and $\frac{d_e^2\boldsymbol{R}'}{dt^2}$, as we know that they compose the primitive features of gestures.

3. Configuration of Accelerometers

Two triaxial MEMS accelerometers can be mounted along the unit's major axis near-symmetrically, as depicted in Fig. 1.

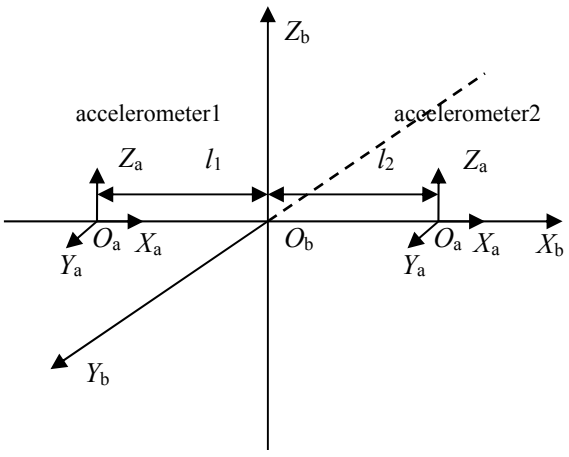

Fig. 1. Configuration scheme of dual MEMS accelerometers.

The body frame $O_bX_bY_bZ_b$ has its origin at the prospective hand-held position and O_bX_b is in direction of the unit's major axis. Two sensors, with all sensitive axes aligned with axis set of body frame, are located on different side of O_b from which the distances to them are $l_1$and l_2. Notice that l_1 is not equal to l_2 usually because the hand-held position may vary at random, but following analysis will prove that this situation doesn't affect the achievement of gestures' features.

When we implement above scheme, two accelerometers can be mounted at the ends of hand-held devices, specific SoC chip with RF interface should be placed at the central position for sampling, calculating, and communication. Because the device is small and narrow just like a pen, holding it by hand is very convenient.

4. Measuring Gestures

For measuring gestures, we need to calculate rotation angular rates, attitude of devices (described with direction cosine matrix), and finally get acceleration of gestures with respect to the local geographic frame. All these tasks can be achieved using specific forces provided by the sensors which allow eqn. (2) to be satisfied.

4.1. Calculating Ground Accelerations

By pre-multiplying both sides of equation (2) by the direction cosine matrix (denoted by C), all the terms can be rewritten with respect to the body frame. We get:

$$\frac{d_b^2 \boldsymbol{R'}}{dt^2} = \frac{d_b^2 \boldsymbol{R}}{dt^2} + \dot{\boldsymbol{\omega}} \times \boldsymbol{L} + \boldsymbol{\omega} \times (\boldsymbol{\omega} \times \boldsymbol{L}) \tag{3}$$

Assuming gravity vector is $\boldsymbol{G}=[0,0,-g]^T$, because the specific forces provided by both accelerometers, $\boldsymbol{F}_1$ and $\boldsymbol{F}_2$, allow following equation to be satisfied:

$$\frac{d_b^2 \boldsymbol{R'}}{dt^2} = \boldsymbol{F} + C^T \boldsymbol{G}, \tag{4}$$

substituting for left item of equation (3) yields:

$$\begin{aligned} \boldsymbol{F}_1 = & \frac{d_b^2 \boldsymbol{R}}{dt^2} + \dot{\boldsymbol{\omega}} \times \boldsymbol{L}_1 \\ & + \boldsymbol{\omega} \times (\boldsymbol{\omega} \times \boldsymbol{L}_1) - C^T \boldsymbol{G} \end{aligned}, \tag{5}$$

and

$$\begin{aligned} \boldsymbol{F}_2 = & \frac{d_b^2 \boldsymbol{R}}{dt^2} + \dot{\boldsymbol{\omega}} \times \boldsymbol{L}_2 \\ & + \boldsymbol{\omega} \times (\boldsymbol{\omega} \times \boldsymbol{L}_2) - C^T \boldsymbol{G} \end{aligned}, \tag{6}$$

where $\boldsymbol{L}_1=[l_1,0,0]^T$, and $\boldsymbol{L}_2=[l_2,0,0]^T$.

Subtracting equation (6) from equation (5) yields:

$$\dot{\boldsymbol{\omega}} \times \boldsymbol{I} = C \frac{\boldsymbol{F}_2 - \boldsymbol{F}_1}{l_1 + l_2} - \boldsymbol{\omega} \times (\boldsymbol{\omega} \times \boldsymbol{I}),$$

where $\boldsymbol{I}=[1,0,0]^T$ is unit vector along axis O_bX_b of the body frame.

Denoting ground acceleration at the position of one of the two accelerometers (for example, accelerometer1, where can be seen as the nib of a pen) by $\boldsymbol{a}$, because following relationship:

$$\frac{d_b^2 \boldsymbol{R}}{dt^2} = C^T \frac{d_e^2 \boldsymbol{R}}{dt^2},$$

is always satisfied, we get:

$$\boldsymbol{a} = C\boldsymbol{F}_1 + \boldsymbol{G}$$

Combining above equations yields:

$$\begin{cases} \boldsymbol{a} = C\boldsymbol{F}_1 + \boldsymbol{G} \\ \dot{\boldsymbol{\omega}} \times \boldsymbol{I} = C \dfrac{\boldsymbol{F}_2 - \boldsymbol{F}_1}{l_1 + l_2} - \boldsymbol{\omega} \times (\boldsymbol{\omega} \times \boldsymbol{I}) \\ \dot{C} = C\Omega \end{cases}, \tag{7}$$

where Ω is the 3×3 matrix, and

$$\Omega = \begin{bmatrix} 0 & -\omega_Z & \omega_Y \\ \omega_Z & 0 & -\omega_X \\ -\omega_Y & \omega_X & 0 \end{bmatrix} \tag{8}$$

Equations (7) indicate that estimating ground accelerations related to gestures relies on the computation of angular rate $\boldsymbol{\omega}$.

4.2. Calculating Angular Rates

Rewriting terms of Equation (7) in component form, namely $\boldsymbol{F}_1=[f_{1X},f_{1Y},f_{1Z}]^T$, $\boldsymbol{F}_2=[f_{2X},f_{2Y},f_{2Z}]^T$, and $\boldsymbol{\omega}=[\omega_X, \omega_Y, \omega_Z]^T$, then the second equation can be expressed as follows:

$$\begin{cases} \dot{\omega}_Y = \dfrac{f_{1Z} - f_{2Z}}{l_1 + l_2} + \omega_X \omega_Z \\ \dot{\omega}_Z = \dfrac{f_{2Y} - f_{1Y}}{l_1 + l_2} + \omega_X \omega_Y \\ \omega_Y^2 + \omega_Z^2 = \dfrac{f_{1x} - f_{2x}}{l_1 + l_2} \end{cases}$$

For each sampling period, terms

$$\frac{f_{1x} - f_{2x}}{l_1 + l_2}, \frac{f_{2Y} - f_{1Y}}{l_1 + l_2}, \frac{f_{1Z} - f_{2Z}}{l_1 + l_2},$$

are all constants. Denoting them by C_X, C_Y, and C_Z respectively yields,

$$\begin{cases} \dot{\omega}_Y = \omega_X \omega_Z + c_Z \\ \dot{\omega}_Z = -\omega_X \omega_Y + c_Y \\ \omega_Y^2 + \omega_Z^2 = c_X \end{cases} \quad (9)$$

The following equation may be derived by differentiating the third item in equation (9):

$$\dot{\omega}_Y \omega_Y + \dot{\omega}_Z \omega_Z = \dot{c}_X / 2, \quad (10)$$

where

$$\dot{c}_X(i) \approx (c_X(i) - c_X(i-1)) / T,$$

in which T is the sampling period.

Substituting for $\dot{\omega}_Y$ and $\dot{\omega}_Z$ in Eqn. (10) gives:

$$c_Z \omega_Y + c_Y \omega_Z = \dot{c}_X / 2$$

Then we get a set of simultaneous equations:

$$\begin{cases} c_Z \omega_Y + c_Y \omega_Z = \dot{c}_X / 2 \\ \omega_Y^2 + \omega_Z^2 = c_X \end{cases} \quad (11)$$

Equation (11) shows that the solution happens to be the intersection of a line and a circle. So ω_Y and ω_Z can be determined as follows:

$$\begin{cases} \omega_Y = \dfrac{\dot{c}_X c_Z \pm c_Y \sqrt{c_X(c_Y^2 + c_Z^2) - \dot{c}_X^2}}{2(c_Y^2 + c_Z^2)} \\ \omega_Z = \dfrac{\dot{c}_X c_Y \mp c_Z \sqrt{c_X(c_Y^2 + c_Z^2) - \dot{c}_X^2}}{2(c_Y^2 + c_Z^2)} \end{cases} \quad (12)$$

Further more, following equation can be derived from equation (9) and (11):

$$\omega_X^2 = ((\dot{\omega}_Y - c_Z)^2 + (\dot{\omega}_Z - c_Y)^2) / c_X,$$

where the symbol of ω_X can be determined according to the angle between following vectors:

$$\boldsymbol{R}_1 = [\omega_Z, -\omega_Y]^T$$
$$\boldsymbol{R}_2 = [\dot{\omega}_Y - c_Z, \dot{\omega}_Z - c_Y]^T$$

Hence ω_X is given by:

$$\omega_X = \mathrm{sgn} \sqrt{\frac{(\dot{\omega}_Y - c_Z)^2 + (\dot{\omega}_Z - c_Y)^2}{c_X}}, \quad (13)$$
$$\mathrm{sgn} = \langle R_1, R_2 \rangle / \left\| \langle R_1, R_2 \rangle \right\|$$

where

$$\begin{cases} \dot{\omega}_Y(i) \approx (\omega_Y(i) - \omega_Y(i-1)) / T \\ \dot{\omega}_Z(i) \approx (\omega_Z(i) - \omega_Z(i-1)) / T \end{cases}$$

According to equation (13), there are two alternative solutions exist. How to determine the unique one can be seen as a function regression problem which refers to tasks of searching the optimum solution in a given space. Considering $\boldsymbol{\omega}$ as a random vector, and defining an energy function:

$$\|\boldsymbol{\omega}\|^2 = \omega_X^2 + \omega_Y^2 + \omega_Z^2$$

Then it is reasonable to assume that solution $\boldsymbol{\omega}_{min}$, which ensures minimizing $\| \boldsymbol{\omega} \|^2$, may be the optimum one. Because relationship $\omega_Y^2+\omega_Z^2=c_X$ is satisfied and c_X is a constant for any sampling period, the objective function $min \| \boldsymbol{\omega} \|^2$ is equivalent to $min\ \omega_X^2$, and then the best estimation of angular velocities can be done by solving the following optimization problem:

$$min\ \omega_X^2$$
$$s.t.$$
$$\begin{cases} \omega_X = sng \sqrt{\dfrac{(\dot{\omega}_Y - c_Z)^2 + (\dot{\omega}_Z - c_Y)^2}{c_X}} \\ \omega_Y = \dfrac{\dot{c}_X c_Z \pm c_Y \sqrt{c_X(c_Y^2 + c_Z^2) - \dot{c}_X^2}}{2(c_Y^2 + c_Z^2)} \\ \omega_Z = \dfrac{\dot{c}_X c_Y \mp c_Z \sqrt{c_X(c_Y^2 + c_Z^2) - \dot{c}_X^2}}{2(c_Y^2 + c_Z^2)} \\ sng = \langle R_1, R_2 \rangle / \left\| \langle R_1, R_2 \rangle \right\| \end{cases}$$

From above analyses, following algorithm for calculating angular rates can be proposed:

For every sampling period, we do:

Step 1: calculate c_X, c_Y, and c_Z from $\mathbf{F}_1$ and $\mathbf{F}_2$;

Step 2: obtain two groups of ω_Y, ω_Z according to equation (12);

Step 3: based on equation (13), two solutions of ω_X are obtained, and then we get two alternative solution vectors: $\boldsymbol{\omega}_1$ and $\boldsymbol{\omega}_2$;

Step 4: from $\boldsymbol{\omega}_1$ and $\boldsymbol{\omega}_2$, the optimum solution is determined by verifying whether the objective function $min\ \omega_X^2$ is satisfied.

4.3. Error Compensation

Normally, zero and random drifts of MEMS accelerometers exist, so there are constant and random errors involved in the values of c_X, c_Y, and c_Z, which will affect the calculating precision of angular

rates. For decreasing these errors, we employ the Kalman stat estimation method to fulfill the error compensation for c_X, c_Y, and c_Z.

Defining stat variable

$$\tilde{C}(t) = (\tilde{c}_X(t), \tilde{c}_Y(t), \tilde{c}_Z(t))^T ,$$

as the actual value corresponding to measured value:

$$C(t) = (c_X(t), c_Y(t), c_Z(t))^T ,$$

then following relationship is satisfied:

$$C(t) = \tilde{C}(t) + E_c(t) + E_r(t) , \quad (14)$$

where $E_c(t)$ and $E_r(t)$ denote constant and random error respectively at time t:

$$E_c(t) = (e_{cX}(t), e_{cY}(t), e_{cZ}(t))^T$$
$$E_r(t) = (e_{rX}(t), e_{rY}(t), e_{rZ}(t))^T$$

Equation (14) is satisfied at time t-1 as well, so,

$$C(t-1) = \tilde{C}(t-1) + E_c(t-1) + E_r(t-1) \quad (15)$$

Combining equation (14) and (15), and rearranging yields:

$$\tilde{C}(t) = \tilde{C}(t-1) + C(t) - C(t-1) + E_c(t-1) - E_c(t) + E_r(t-1) - E_r(t)$$

For constant errors, $E_c(t)$- $E_c(t\text{-}1)$=0 are always satisfied; meanwhile the difference between two white Gaussian noise signals is still white Gaussian noise. So we assume $W(t)$=$E_r(t\text{-}1)$- $E_r(t)$, the above equation can be written as follows:

$$\tilde{C}(t) = \tilde{C}(t-1) + C(t) - C(t-1) + W(t) , \quad (16)$$

which is the system state equation.

Because

$$E_c(t) \approx \sum_{i=1}^{N} C(i) / (N * T) ,$$

if we assume

$$Y(t) = C(t) - E_c(t) ,$$

the system measurement equation can be derived:

$$Y(t) = \tilde{C}(t) + E_r(t) \quad (17)$$

According to equation (16) and (17), the optimum estimations of c_X , c_Y, and c_Z can be achieved by executing Kalman filtering algorithm.

5. Experimental Analyses

In order to verify above scheme of dual accelerometers and related algorithms, we conducted an evaluation of calculating precision about angular rates under noise-free and noise environment and experiments of gesture-based figure recognition.

5.1. Angular Rates Regression Tests

Assuming gesture satisfies the following model:

$$\begin{cases} \omega_x(t) = 1.5\sin(5t) \\ \omega_y(t) = 2\cos(4t) - 2 \\ \omega_z(t) = 2 * \sin(3t) \end{cases} ,$$

$$\begin{cases} a_x(t) = 3\sin(12t) \\ a_y(t) = 3\cos(8t)\cos(4t) \\ a_z = 4\cos(8t)\cos(2t) \end{cases}$$

where angular rates and accelerations are measured in rad/s and m/s^2 respectively, l_1= l_2=0.04m, sampling period is 5 ms. The fitting curve between calculated and real angular rates along X, Y, and Z axis are depicted in Fig. 2, Fig. 3, and Fig. 4.

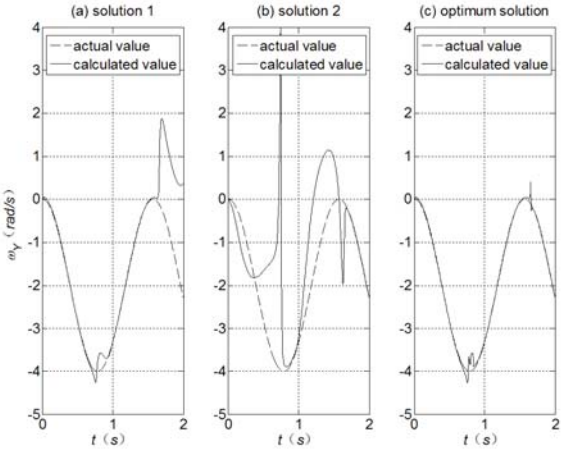

Fig. 2. ω_Y resolving deviation.

From Fig. 2 and Fig. 3, we can see that ω_Y and ω_Z can be rebuilt accurately (Fig. 2 (c), Fig. 3 (c)) from two alternatives (Fig. 2 (a), Fig. 2 (b), Fig. 3 (a), and Fig. 3 (b)). At very few points along time axis, disagreements between estimated and real values exist, this is caused by calculating errors (referring to Eqn. (12), if denominator becomes zero, namely $\omega_Y^2+\omega_Z^2 \rightarrow 0$, errors will increase).

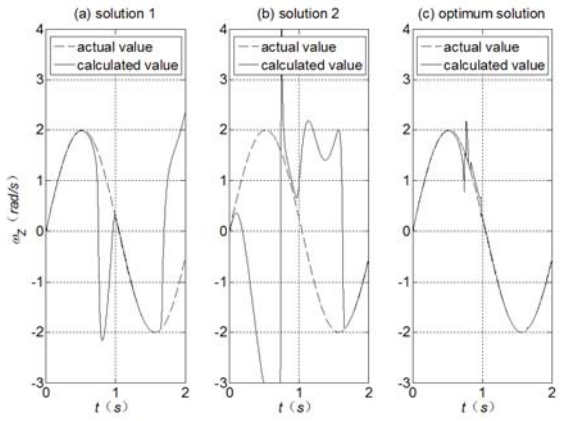

Fig. 3. ω_Z resolving deviation.

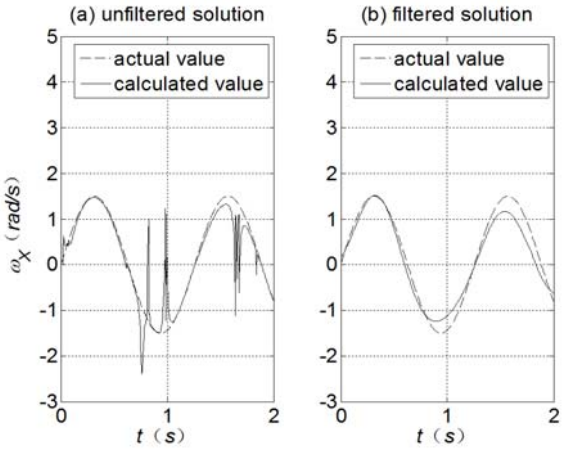

Fig. 4. ω_X resolving deviation.

Fig. 4 (a) shows that calculating errors of ω_X are bigger than ω_Y and ω_Z. Comparing with Fig. 2 and Fig. 3, we can find the points at which errors exist consist with where errors of ω_Y and ω_Z appear. This can be attributed to the calculating process of ω_X, which relies on the derivative of ω_Y and ω_Z, namely, little error of ω_Y and ω_Z will result in bigger one after derivation. Because these points are sparse, corresponding errors can be eliminated as the high frequency-segments by low pass filtering. The final result fits actual value well (Fig. 4 (b)).

5.2. Gestures Tracks Recovering Tests

For the further performance determination of related methods presented in section 3 and 4 under noise environments, we made a figure-aimed recognition test based on our methods.

Preparing the evaluation we use Nintendo Wii Motion Plus Wireless Controller as our input device [13], which incorporates a triaxial MEMS accelerometer, a dual-axis tuning fork gyro and a single-axis gyro. Connected to PC instead of gaming console via the Bluetooth Human Interface Device (HID) protocol, It is possible to readout all sensors' data (which has been reverse engineered by the open-source community).

For implementing our scheme, we butt two Wii Controller together along their major axis. According to the physical placement, two accelerometers are 0.12 m apart with all sensitive axes aligned. As extra components, gyro sensors are used to verify the precision of calculated angular rates, and trigger-style button B on the back of the controller is used to trigger and stop the sampling procedures (which approximately keep active for 2 seconds). Related algorithms of computing gestures' tracks are implemented in Matlab environment.

In accordance with the methods described in section 3, we firstly execute Kalman filtering algorithm, and then calculate angular rates and compare which with gyro outputs.

Fig. 5 shows the fitting curve between measured, estimated values of c_X, c_Y, and c_Z and ideal ones calculated based on gyro outputs when we write '8' with gesture. It can be seen that the fitting curves of estimated data are well consonant with what calculated from gyro outputs, which proves the system state & measurement equations are effective.

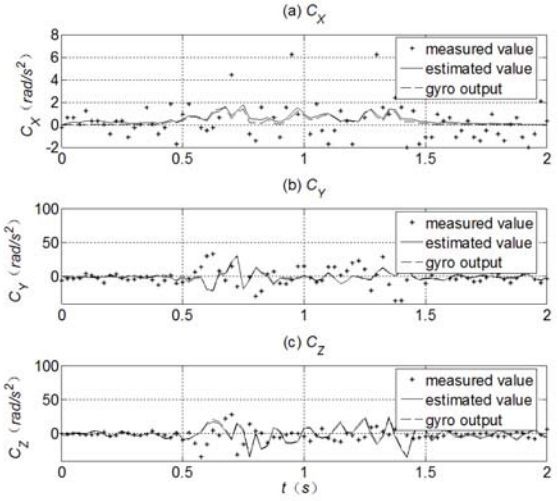

Fig. 5. Effects of Kalman state estimation.

Table 1 lists correlation coefficients between calculated angular rates and gyro outputs with regard to gestures about figures 0-9. Results show that they are highly correlated (for all figures, r>0.85), which indicates the combination of filtering and succedent resolving algorithms work well. Furthermore, we can see that correlation degrees about ω_X are lower than about ω_Y and ω_Z, which can be attributed to derivation operations, this is consistent with the conclusions in section 5.1.

For observing gestures' tracks of figures 0-9, we firstly get direction cosine matrix by integrating angular rates, linear accelerations, and then three-dimensional tracks, subsequently the planar tracks are achieved by executing dimensionality reduction with PCA-based methods [14], which are shown in Fig. 6.

Results show that there are some adjoining or distortional strokes in these tracks because no references and feedbacks exist among gesture processes, but they are sufficient grounds for subsequent pattern recognitions.

Table 1. Correlation coefficients between resolving and gyroscope sampling values.

Char	ω_X	ω_Y	ω_Z
0	0.8764	0.9218	0.9196
1	0.9102	0.9523	0.9438
2	0.8521	0.9176	0.9027
3	0.8568	0.9133	0.9273
4	0.8625	0.9189	0.9107
5	0.8806	0.9217	0.9087
6	0.8795	0.9201	0.9115
7	0.9015	0.9350	0.9176
8	0.8912	0.9298	0.9182
9	0.8897	0.9137	0.9208

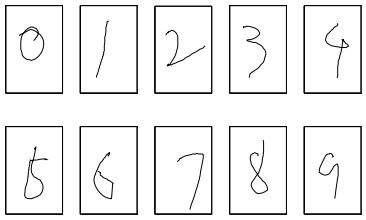

Fig. 6. Gesture traces of figures.

6. Conclusions

In this paper, we proposed a design of micro inertial measurement unit for gesture-based interface, which is characterized by the configuration of dual MEMS accelerometers, and the algorithm for calculating angular rates and linear accelerations. The near-symmetrical layout of two triaxial MEMS accelerometers promises the unit is small and convenient for holding; meanwhile, corresponding algorithm has simple form for calculating angular rates, by using an energy function, we can achieve an estimation of time series about angular rates accurately. Due to analytic instead of integration methods, cumulative errors are not involved in calculating angular rates process; Kalman filtering for arguments denoising contributes to improve resolving precision further. Preliminary experimental verification shows that all these scheme and methods are reasonable and feasible.

References

[1]. Sushmita Mitra, Tinku Acharya, Gesture recognition: a survey, *IEEE Transactions on System, Man, and Cybernetics*, Vol. 37, Issue 3, 2007, pp. 311-324.

[2]. I. J. Jang, W. B. Park, Signal processing of the accelerometer for gesture awareness on handheld devices, in *Proceedings of the IEEE International Workshop on Robot and Human Interactive Communication, Roman'2003*, 31 October – 2 November 2003, pp. 139-144.

[3]. J. Kela, P. Korpipaa, D. Marca, Accelerometr-based gesture control for a design environment, *Personal and Ubiquitous Computing*, Vol. 10, Issue 5, 2005, pp. 258-299.

[4]. Sven Kratz, Michael Rohs, Georg Essl, Combining acceleration and gyroscope data for motion gesture recognition using classifiers with dimensionality constraints, in *Proceedings of the International Conference on Intelligent User Interfaces (IUI'13)*, Santa Monica, USA, 19-22 March 2013, pp. 173-178.

[5]. Thomas Schlomer, Benjamin Poppinga, Niels Henze and Susanne Boll, Gesture recognition with a Wii controller, in *Proceedings of the 2nd International Conference on Tangible and Embedded Interaction (TEI'08)*, Bonn, Germany, 18-21 February 2008, pp. 11-14.

[6]. L. D. DiNapoli, The measurement of angular velocities without the use of gyros, *The Moore School of Electrical Engineering, University of Pennsylvania*, Philadelphia, 1965.

[7]. A. R. Schuler, Measuring rotational motion with linear accelerometers, *IEEE Transactions on Aerospace and Electronic Systems*, Vol. 3, Issue 3, 1967, pp. 465-472.

[8]. S. J. Merhav, A nongyroscopic inertial measurement unit, *Journal of Guidance, Control, and Dynamics*, Vol. 5, Issue 3, 1982, pp. 227-235.

[9]. Sou-Chen Lee, Liu Cheng-Yu, An innovative estimation method with own-ship estimator for an all accelerometer-type inertial navigation system, *International Journal of Systems Science*, Vol. 30, Issue 12, 1999, pp. 1259-1266.

[10]. Yue Peng, Shi Zhen, Gyro free inertial navigation system based on MEMS accelerometer, *Journal of Chinese Inertial Technology*, Vol. 19, Issue 2, 2011, pp. 152-156.

[11]. Xue Yang, Jin Lian-Wen, A feature extraction and recognition approach for accelerometer based virtual handwriting digit, *Pattern Recognition and Artificial Intelligence*, Vol. 24, Issue 4, 2011, pp. 492-500.

[12]. Xue Yang, Human motion patterns recognition based on single triaxial accelerometer, *School of Electronic and Information Engineering, South China University of Technology*, Guangzhou, 2011.

[13]. Nintendo Web Portal (http://wii.nintendo.com).

[14]. Ian Jolliffe, Principal component analysis, Brian Everitt, *John Wiley & Sons*, 2005.